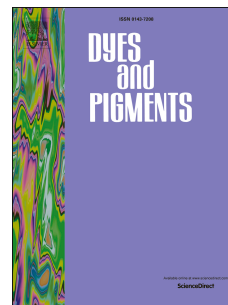


Accepted Manuscript

Benzotriazole-containing donor-acceptor-acceptor type cyclometalated iridium(III) complex for solution-processed near-infrared polymer light emitting diodes

Junting Yu, Hua Tan, Fanyuan Meng, Kun Lv, Weiguo Zhu, Shijian Su



PII: S0143-7208(16)30142-5

DOI: [10.1016/j.dyepig.2016.04.021](https://doi.org/10.1016/j.dyepig.2016.04.021)

Reference: DYPI 5199

To appear in: *Dyes and Pigments*

Received Date: 9 January 2016

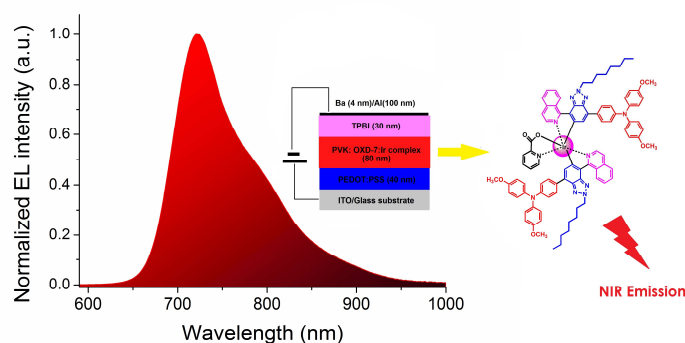
Revised Date: 7 April 2016

Accepted Date: 9 April 2016

Please cite this article as: Yu J, Tan H, Meng F, Lv K, Zhu W, Su S, Benzotriazole-containing donor-acceptor-acceptor type cyclometalated iridium(III) complex for solution-processed near-infrared polymer light emitting diodes, *Dyes and Pigments* (2016), doi: 10.1016/j.dyepig.2016.04.021.

This is a PDF file of an unedited manuscript that has been accepted for publication. As a service to our customers we are providing this early version of the manuscript. The manuscript will undergo copyediting, typesetting, and review of the resulting proof before it is published in its final form. Please note that during the production process errors may be discovered which could affect the content, and all legal disclaimers that apply to the journal pertain.

Graphical Abstract



A novel benzotriazole-containing donor-acceptor-acceptor type cyclometalated iridium(III) complex of $(\text{CH}_3\text{OTPA-BTz-Iq})_2\text{Irpic}$ was synthesized. Using it as a dopant and a blend of PVK and OXD-7 as a host matrix, the PLEDs exhibited a near-infrared (NIR) emission peaked at 723 nm and a shoulder at 780 nm with the maximum *EQE* of 0.41% at 8.14 mA cm^{-2} . This work indicates that introducing appropriate D and A unit to develop D-A-A structure is an efficient approach to construct near-infrared-emitting iridium(III) complex and obtain high-efficiency near-infrared polymer light-emitting diodes with suppressive efficiency roll-off.

Benzotriazole-containing Donor-Acceptor-Acceptor Type Cyclometalated
Iridium(III) Complex for Solution-processed Near-infrared Polymer Light
Emitting Diodes

Junting Yu,^{a*} Hua Tan,^b Fanyuan Meng,^b Kun Lv,^a Weiguo Zhu,^{b*} and Shijian Su^{c*}

^a Key Laboratory of Theoretical Organic Chemistry and Functional Molecule,
Ministry of Education, College of Chemistry and Chemical Engineering, Hunan
University of Science and Technology, Xiangtan 411201, P. R. China

^b College of Chemistry, Key Lab of Environment-Friendly Chemistry and Application
in the Ministry of Education, Xiangtan University, Xiangtan 411105, P. R. China

^c Institute of Polymer Optoelectronic Materials and Devices, South China University
of Technology, Guangzhou 510640, P. R. China

Corresponding author: Dr. Junting Yu

Prof. Weiguo Zhu

Prof. Shijian Su

Tel: +86-731-58290097

E-mail addresses: yujuntingtt@163.com

zhuwg18@126.com

Abstract: A novel near-infrared-emitting cyclometalated iridium(III) complex of (CH₃OTPA-BTz-Iq)₂Irpic containing benzotriazole unit with a donor-acceptor-acceptor (D-A-A) chromophore was synthesized and characterized. The optophysical, electrochemical and electroluminescent characteristics were primarily studied. A near-infrared emission peaked at 716 nm with a shoulder at 790 nm was exhibited in the (CH₃OTPA-BTz-Iq)₂Irpic dichloromethane solution at 298 K. In its optimized solution-processed polymer light-emitting diodes, a near-infrared electroluminescent emission peaked at 723 nm with a shoulder at 780 nm was observed with a maximum external quantum efficiency of 0.41% at 8.14 mA cm⁻². This work indicates that introducing appropriate D and A units to develop D-A-A structure is an efficient approach to construct near-infrared-emitting iridium(III) complex in the polymer light-emitting diodes with suppressive efficiency roll-off.

Keywords: donor-acceptor-acceptor; iridium(III) complexes; benzotriazole; near-infrared emission; electrophosphorescence; polymer light-emitting devices

1. Introduction

With the rapid development of organic light-emitting diodes (OLEDs) in recent years, the research on near-infrared (NIR)-OLEDs has gained great attentions for diverse potential applications in night-vision-readable displays, sensors, optical communication and medical systems [1-5]. To date, the developed organic NIR-emitting materials mostly contain lanthanide complexes [6-8], fluorescent materials with a donor-acceptor (D-A) structure [9-14], boron dipyrromethene dyes [15-20] and transition-metal complexes [21-34]. Therein, phosphorescent transition-metal complexes using osmium(II), iridium(III) or platinum(II) as the metal center are available to exhibit higher emission efficiency due to their strong spin-orbit coupling in the presence of heavy metal atoms, which leads to an internal quantum efficiency as high as 100% [35,36]. For example, in a device with a sophisticated configuration, the platinum(II) complex of PtL²Cl realized a maximum external quantum efficiency (EQE_{\max}) of 14.5% at ~700 nm, which is the highest value for these NIR devices to date [22]. However, these EQE levels were typically obtained from excimers emission, the performance and the reproducibility of the devices cannot be well controlled [37]. Platinum (II) porphyrins are also the most typical NIR emission materials in the reported transition metal complexes and have exhibited an EQE maxima of 2.49% for polymer light-emitting devices (PLEDs) and 9.2% for OLEDs with NIR emission in the 760-780 nm range. However, these EQE levels were typically obtained at very low current densities. In high current densities, the devices exhibit a significant EQE roll-off, which could be attributed to the increasing triplet-triplet exciton annihilation and aggravated by long excited-state lifetimes in the planar-square platinum(II) phosphors [25].

In contrast to the planar-square platinum (II) complexes, iridium (III) complexes

with typical octahedral configuration, relatively short triplet lifetime and high phosphorescent efficiency have the ability to effectively prevent intermolecular aggregation-induced emission (AIE) quenching and significantly alleviate the efficiency roll-off in OLEDs [29]. In order to develop new NIR-emitting iridium (III) complexes, many researchers have made some contributions to this field. The earlier NIR-emitting example of iridium (III) bis(1-pyrenyl-isoquinolino-N,C') acetylacetonate was reported by Williams *et al.* in 2006, which displayed an electroluminescence (EL) emission peaked at 720 nm with an EQE_{\max} nearly 0.1% [20]. Recently, Qiu *et al.* reported a series of the NIR-emitting iridium (III) phosphors [27-29], in which an iridium (III) emitter of $\text{Ir}(\text{pbq-g})_2(\text{Bphen})$ exhibited an extended emission peak at 850 nm by introducing an sp^2 -hybridized N atom opposite the chelating N atom in the phenylbenzoquinoline (pbq) ligand [28]. The $\text{Ir}(\text{pbq-g})_2(\text{Bphen})$ based devices achieved a maximum EQE up to 2.2% with negligible efficiency roll-off. In 2015, an iridium(III) phosphor of $(\text{thdpqx})_2\text{Ir}(\text{acac})$ (dpqx= diphenylquinoxaline, th=thienyl) was reported and exhibited an EL emission peak at 704 nm in its doped devices with an EQE_{\max} of 3.4% [31], which is the highest value for the NIR-emitting devices based on cyclometalated iridium (III) complexes to date.

It's worth noting that some NIR-emitting organic and polymeric fluorescent materials with D-A chromophores have been developed because the band gap levels and photoelectronic properties can be readily tuned through a systematic variation between the D and A units [9-14]. According to this idea, introduction of the D-A structure into phosphorescent materials should be expected to achieve NIR emission with better device performance. In 2013, Wong *et al.* reported a series of cyclometalated iridium (III) complexes with functionalized borylated oligothiophene ligands and their maximum emission peaks extended to 756 nm. However, the EQE maximum

is merely 0.07% as the strong D-A interaction triggered a much faster radiationless decay, and the EL spectrum exhibited a dual emission, which indicates that the energy transfer from the host exciton to the phosphor is not completely [30]. The similar phenomenon was also occurred in our previous research. In 2014, our group reported a D-A-A type cyclometalated platinum (II) complex (TPA-BT-Q)Ptpic with a functionalized cyclometalated ligand of triphenylamine (TPA)-benzothiadiazole (BT)-quinoline (Q). The devices exhibited a maximum emission peak at 760 nm, and the EQE_{\max} is only 0.12% [38]. Therefore, selecting the appropriate D and A units is the main subject.

Inspired by the works mentioned above, we here designed a novel benzotriazole-containing D-A-A type cyclometalated iridium (III) complex of (CH₃OTPA-BTz-Iq)₂Irpic, in which methoxy-triphenylamine (CH₃OTPA) is used as an electron-donating unit, an alkylbenzotriazole (BTz) and an isoquinoline (Iq) are employed as electron-withdrawing units and the alky group is introduced in order to improve molecular solubility (Figure 1). In this complex, non-planar CH₃OTPA unit is available to improve carrier-transporting properties and overcome the aggregation-induced emission quenching; the BTz unit is an acceptor with moderate electron-withdrawing intensity (compared with the benzothiadiazole) due to the substitution of the sulfur atom in benzothiadiazole with a nitrogen atom, which may reduce the intensity of D-A interaction and suppress the nonradiative transition to some extent [39]. Besides, BTz is a good class of EL materials reported in recent years [40-43], the lone pair on the nitrogen atom is more basic than the lone pair on sulfur and is more easily donated into the triazole ring [39]. This is also contributed to form a more stable complex. The synthetic route of (CH₃OTPA-BTz-Iq)₂Irpic is shown in Scheme 1. To prove our tactics, we comprehensively studied its thermal, photophysical, and electrochemical

properties, further EL properties of its doped PLEDs by a solution process. In the optimized solution-processed phosphorescent PLEDs, a NIR EL emission peaked at 723 nm with a shoulder at 780 nm was observed. An *EQE* maximum of 0.41% at 8.14 mA cm⁻² was obtained in the (CH₃OTPA-BTz-Iq)₂Irpic doped devices. This work indicates that introducing appropriate D and A units to develop D-A-A structure is an efficient approach to construct high-efficiency NIR-emitting iridium (III) complex in PLEDs with suppressive efficiency roll-off.

2 Experimental

2.1 Characterization

The solvents were carefully dried and distilled by standard procedures before use. All chemicals, unless otherwise stated, were obtained from commercial sources and used as received. ¹H NMR spectra was recorded with a Bruker Dex-400 NMR instrument using CDCl₃ as a solvent. Elemental analysis was carried out with a vario EL III elemental analysis instrument. Mass spectrum was recorded on a Bruker auto-flexIII smartbeam MALDI-TOF spectrometer. Ultraviolet-visible (UV-vis) absorption and photoluminescent (PL) spectra at 298 K were recorded with a PE Lambda 25 spectrophotometer and a PTI Q40 luminescence spectrometer, respectively. PL spectra at 77 K were recorded with Edinburgh analytical instrument (FLS920 fluorescence spectrometer). Lifetime studies both at 77 K and 298 K were performed by an Edinburgh FLS920 transient spectrofluorimeter with time-correlated single-photon counting technique at the peak PL wavelength. The equation of $\Phi_s = \Phi_r(\eta_s^2 A_r I_s / \eta_r^2 A_s I_r)$ was used to calculate the fluorescence quantum yield (Φ) of the iridium(III) complex using complex Ru(bpy)₃(PF₆)₂ as the standard compound in N₂ atmosphere, where Φ_s is the quantum yield of the sample, Φ_r is the quantum yield of the reference, η is the

refractive index of the solvent, A_s and A_r are the absorbance of the sample and the reference at the wavelength of excitation, I_s and I_r are the integrated areas of emission bands [44]. Thermogravimetric analysis (TGA) was conducted under a dry nitrogen gas flow at a heating rate of $20^\circ\text{C min}^{-1}$ on a TA TQAQ50 instrument. Cyclic voltammetry was performed on a CHI 600E electrochemical work station with a scan rate of 100 mV S^{-1} at room temperature under argon, in which a Pt disk, Pt plate and Ag/AgCl electrode were used as working electrode, counter electrode and reference electrode in $n\text{-Bu}_4\text{NPF}_6$ (0.1 M) acetonitrile solution, respectively. For calibration, the redox potential of ferrocene/ferrocenium (Fc/Fc^+) was measured under the same conditions.

2.2 PLEDs Fabrication and Measurement

Patterned indium tin oxide (ITO)-coated glass substrates with a sheet resistance of $15\text{-}20 \Omega \text{ square}^{-1}$ underwent a wet-cleaning course in an ultrasonic bath, beginning with THF, following by isopropanol, detergent, deionized water and isopropanol, respectively. After oxygen-plasma treatment, a 40 nm thick anode hole-injection layer of poly(ethylenedioxythiophene):poly(styrene-sulfonate) (PEDOT:PSS, Baytron P 4083, Bayer AG) film was spin-cast on the ITO substrate and dried by baking in vacuum oven at 120°C for 20 min. The 80 nm emitting layer was prepared by spin-coating from chlorobenzene solution on the top of PEDOT:PSS layer, then annealed at 120°C for 20 min to remove the solvent residue. Finally, an electron transfer layer of TPBI (30 nm), a cathode composed of Ba (4 nm) and Al (100 nm) layer was evaporated with a shadow mask at a base pressure of $1 \times 10^{-4} \text{ Pa}$. The thickness of the evaporated cathode was monitored by a quartz crystal thickness /ratio monitor (Model: STM-100/MF, Sycon). The overlapping area between the cathode and anode defined a pixel size of 15 mm^2 . Except for the spin coating of the PEDOT:PSS layer, all the

fabrication processes were carried out inside a controlled atmosphere of nitrogen dry-box (Vacuum Atmosphere Co.) containing less than 1 ppm oxygen and moisture. All measurements were carried out at room temperature (RT) under ambient conditions. The *J-V* characteristics were measured using a Keithley 236 source measurement unit and a calibrated silicon photodiode. Radiant emittance values were calculated assuming a Lambertian distribution accordingly. The external quantum efficiency values were calculated from the current density, luminance and EL spectrum, assuming a Lambertian distribution. The EL spectra were obtained by using miniature fiber optic spectrometer (USB 2000, Ocean Optics).

2.3 Syntheses

2.3.1 Synthesis of *N*-(4-bromophenyl)-4-methoxy-*N*-(4-methoxyphenyl)benzenamine (1)

A mixture of 1-iodo-4-methoxybenzene (10.00 g, 42.74 mmol), 4-bromobenzeneamine (2.95 g, 17.15 mmol) and 1,10-phenanthroline anhydrous (0.62 g, 3.42 mmol) in toluene (60 mL) was heated and stirred under nitrogen atmosphere. When the temperature reached to 110 °C, the CuI (0.65 g, 3.42 mmol) and KOH (7.66 g, 136.79 mmol) were added quickly, and then the mixture was stirred at 135 °C for 12 h. After cooled to RT, the mixture was poured into distilled water (50 mL) and extracted with dichloromethane (DCM) (3×30 mL). The combined organic layer was dried over MgSO₄ for 2 h and filtrated. The filtrate was concentrated by rotary evaporator under reduced pressure. The residue was purified by silica gel column chromatography using DCM/ petroleum ether (PE) (1/5, V/V) as eluent to gain lyard powder (4.63 g, 70.4%). ¹H NMR (400 MHz, CDCl₃, ppm): 7.25 (d, *J* = 4.0 Hz, 2H), 7.04 (d, *J* = 8.4 Hz, 4H), 6.83 (d, *J* = 8.2 Hz, 6H), 3.79 (s, 6H).

2.3.2 Synthesis of 4-methoxy-*N*-(4-methoxyphenyl)-*N*-(4-(4,4,5,5-tetramethyl-1,3,2-dioxaborolan-2-yl)phenyl)benzenamine (2)

A mixture of compound **1** (2.03 g, 5.28 mmol), 4,4,5,5-tetramethyl-2-(4,4,5,5-tetramethyl-1,3,2-dioxaborolan-2-yl)-1,3,2-dioxaborolane (5.34 g, 21.12 mmol), potassium acetate (2.58 g, 26.38 mmol) and [1,1'-bis(diphenylphosphino)ferrocene]dichloropalladium (II) (0.12 g, 0.16 mmol) in DMSO (65 mL) was heated and stirred at 80 °C under nitrogen atmosphere for 20 h. After cooled to RT, the mixture was poured into distilled water (50 mL) and extracted with DCM (3×30 mL). The combined organic layer was washed with distilled water (4×40 mL) and dried over MgSO₄ for 2 h and filtrated. The filtrate was concentrated by rotary evaporator under reduced pressure. The residue was purified by silica gel column chromatography using DCM/PE (1/1, V/V) as eluent to gain lyard powder (1.40 g, 61.5%). ¹H NMR (400 MHz, CDCl₃, ppm): 7.60 (d, *J* = 7.0 Hz, 2H), 7.07 (d, *J* = 6.0 Hz, 4H), 6.84 (d, *J* = 8.0 Hz, 6H), 3.79 (s, 6H), 1.32 (s, 12H).

2.3.3 Synthesis of *N*-(4-(7-bromo-2-octyl-2H-benzo[d][1,2,3]triazol-4-yl)phenyl)-4-methoxy-*N*-(4-methoxyphenyl)benzenamine (**3**)

A mixture of compound **2** (1.00 g, 2.32 mmol), 4,7-dibromo-2-octyl-2H-benzo[d][1,2,3]triazole (1.17 g, 3.14 mmol), Na₂CO₃ (6 mL, 2M), Pd(PPh₃)₄ (80 mg, 0.07 mmol) in toluene (25 mL) and methanol (6 mL) was heated and stirred at 80 °C under nitrogen atmosphere for 12 h. After cooled to RT, the mixture was poured into distilled water (50 mL) and extracted with DCM (3×30 mL). The combined organic layer was dried over MgSO₄ for 2 h and filtrated. The filtrate was concentrated with rotary evaporator under reduced pressure. The residue was purified by silica gel column chromatography using DCM/PE (1/2, V/V) as eluent to gain light yellow powder (0.78 g, 55.6%). ¹H NMR (400 MHz, CDCl₃, ppm): 7.86 (d, *J* = 8.6 Hz, 2H), 7.60 (d, *J* = 7.2 Hz, 1H), 7.37 (d, *J* = 7.6 Hz, 1H), 7.14 (d, *J* = 8.8 Hz, 4H), 7.04 (d, *J* = 8.4 Hz, 2H), 6.87 (d, *J* = 8.8 Hz, 4H), 4.78 (t, *J* = 7.2 Hz, 2H), 3.81 (s, 6H),

2.16-2.12 (m, 2H), 1.36-1.25 (br, 10H), 0.87 (t, $J = 6.4$ Hz, 3H). MALDI-TOF MS (m/z) for $C_{34}H_{37}BrN_4O_2$, Calcd: 612.210, Found, 612.232.

2.3.4 Synthesis of 4-methoxy-*N*-(4-methoxyphenyl)-*N*-(4-(2-octyl-7-(4,4,5,5-tetramethyl-1,3,2-dioxaborolan-2-yl)-2H-benzo[d][1,2,3]triazol-4-yl)phenyl)benzenamine (**4**)

A mixture of compound **3** (0.26 g, 0.43 mmol), 4,4,5,5-tetramethyl-2-(4,4,5,5-tetramethyl-1,3,2-dioxaborolan-2-yl)-1,3,2-dioxaborolane (0.42g, 1.68mol), potassium acetate (0.33 g, 3.36 mmol) and [1,1'-bis(diphenylphosphino) ferrocene] dichloropalladium (II) (52 mg, 0.07 mmol) in anhydrous tetrahydrofuran (50 mL) was heated and stirred at 65 °C under nitrogen atmosphere for 12 h. After cooled to RT, the mixture was poured into distilled water (50 mL) and extracted with DCM (3×30 mL). The combined organic layer was dried over $MgSO_4$ for 2 h and filtrated. The filtrate was concentrated by rotary evaporator under reduced pressure. The residue was purified by silica gel column chromatography using DCM/PE (1/1, V/V) as eluent to gain yellow viscous compound (0.21 g, 73.5%). 1H NMR (400 MHz, $CDCl_3$, ppm): 7.95-7.93 (m, 3H), 7.51 (d, $J = 7.2$ Hz, 1H), 7.13 (d, $J = 8.8$ Hz, 4H), 7.04 (d, $J = 8.8$ Hz, 2H), 6.86 (d, $J = 8.8$ Hz, 4H), 4.78 (t, $J = 7.6$ Hz, 2H), 3.81 (s, 6H), 2.16-2.12 (m, 2H), 1.42-1.40 (br, 10H), 1.26 (s, 12H), 0.88 (t, $J = 4.2$ Hz, 3H). MALDI-TOF MS (m/z) for $C_{40}H_{49}BN_4O_4$, Calcd: 660.385, Found, 660.392.

2.3.5 Synthesis of the **CH₃OTPA-BTz-BT-Iq** ligand

A mixture of compound **4** (0.15 g, 0.23 mmol), 1-bromoisoquinoline (52 mg, 0.25 mmol), K_2CO_3 (2 mL, 2M), $Pd(PPh_3)_4$ (7 mg, 0.01 mmol) in toluene (18 mL) and methanol (2 mL) was heated and stirred at 80 °C under nitrogen atmosphere for 24 h. After cooled to RT, the mixture was poured into distilled water (15 mL) and extracted with DCM (3×15 mL). The combined organic layer was dried over $MgSO_4$ for 2 h and filtrated. The filtrate was concentrated by rotary evaporator under reduced pressure.

The residue was purified by silica gel column chromatography using DCM as eluent to gain yellow solid (0.13 g, 86.5%). ^1H NMR (400 MHz, CDCl_3 , ppm): 8.71 (d, $J = 5.6$ Hz, 1H), 7.99-7.91 (m, 4H), 7.74-7.66 (m, 4H), 7.50 (t, $J = 3.0$ Hz, 1H), 7.17 (d, $J = 8.4$ Hz, 4H), 7.09 (d, $J = 8.0$ Hz, 2H), 6.89 (d, $J = 8.4$ Hz, 4H), 4.71 (t, $J = 7.0$ Hz, 2H), 3.82 (s, 6H), 2.06-2.02 (m, 2H), 1.31-1.22 (br, 10H), 0.84 (t, $J = 3.8$ Hz, 3H). MALDI-TOF MS (m/z) for $\text{C}_{43}\text{H}_{43}\text{N}_5\text{O}_2$, Calcd: 661.342, Found, 661.465.

2.3.6 Synthesis of $(\text{CH}_3\text{OTPA-BTz-Iq})_2\text{Irpc}$

A mixture of $\text{IrCl}_3 \cdot \text{H}_2\text{O}$ (30 mg, 0.09 mmol), $\text{CH}_3\text{OTPA-BTz-Iq}$ (150 mg, 0.23 mmol), 2-ethoxyethanol 12 mL and distilled water 4 mL was stirred under nitrogen atmosphere at 100 °C for 24 h. After cooled to RT, the mixture was poured into distilled water (15 mL) and extracted with DCM (3×15 mL). The combined organic layer was dried over Na_2SO_4 for 4 h and filtrated. The filtrate was concentrated with rotary evaporator under reduced pressure to gain the violet chloro-bridged precursor.

The dried chloro-bridged precursor (139 mg, 0.045 mmol) was mixed with 2-ethoxyethanol (15 mL), picolinic acid (44 mg, 0.36 mmol) and anhydrous Na_2CO_3 (30 mg, 0.28 mmol). The resulting mixture was stirred under nitrogen atmosphere at 110 °C for 24 h. After cooling to RT, the resulting precipitate was filtered off and washed with water, ethanol and hexane, respectively. The residue was purified by silica gel column chromatography using DCM/ethyl acetate (EA) ($V/V=3/1$) as eluent to get an orange powder (31 mg, 41.7 %). ^1H NMR (400 MHz, CDCl_3 , ppm): 9.76 (d, $J = 8.0$ Hz, 1H), 9.59 (d, $J = 8.0$ Hz, 1H), 8.78 (d, $J = 6.4$ Hz, 1H), 8.34 (d, $J = 7.6$ Hz, 1H), 7.88-7.80 (m, 4H), 7.68-7.63 (m, 6H), 7.55 (d, $J = 6.4$ Hz, 1H), 7.45-7.39 (m, 4H), 7.31 (d, $J = 7.8$ Hz, 2H), 7.23 (d, $J = 6.6$ Hz, 1H), 7.03-7.00 (m, 8H), 6.83 (d, $J = 7.4$ Hz, 8H), 6.74 (d, $J = 9.4$ Hz, 2H), 6.67 (d, $J = 8.2$ Hz, 2H), 6.35 (s, 1H), 4.64 (t, $J = 5.6$ Hz, 4H), 3.80 (s, 12H), 2.14-2.05 (m, 4H), 1.43-1.26 (br, 20H), 0.84 (t, $J = 5.6$

Hz, 6H). MALDI-TOF MS (m/z) for $C_{92}H_{88}IrN_{11}O_6$, Calcd: 1635.655, Found, 1635.803. Anal. Calc. for $C_{92}H_{88}IrN_{11}O_6$: C 67.54, H 5.42, N 9.42% Found: C 67.21, H 5.34, N 9.27%

3. Results and Discussion

3.1 Synthesis and thermal stability

Compound **3** and $CH_3OTPA-BTz-Iq$ were synthesized through Suzuki couplings. The $(CH_3OTPA-BTz-Iq)_2Irpic$ was synthesized using the previous method with two-step procedures, which contain a cyclometalation of $CH_3OTPA-BTz-Iq$ and a cleavage of the chloride groups in the corresponding dimers with picolinic acid. The $(CH_3OTPA-BTz-Iq)_2Irpic$ was characterized by 1H NMR, MALDI-TOF mass spectra and element analysis.

Thermal property of $(CH_3OTPA-BTz-Iq)_2Irpic$ was characterized by TGA. The recorded TGA curve is shown in Figure S1 (see Electronic Supporting Information, ESI). The onset decomposition temperature for 5 % weight loss (T_d) was 302 °C, which indicates the $(CH_3OTPA-BTz-Iq)_2Irpic$ has high thermal stability.

3.2 Photophysical Properties

The photophysical properties of $(CH_3OTPA-BTz-Iq)_2Irpic$ in DCM solution were investigated at 298 K (Table 1). Figure 2 shows the UV-vis spectrum of $(CH_3OTPA-BTz-Iq)_2Irpic$. For comparison, the UV-vis spectrum of the $CH_3OTPA-BTz-Iq$ ligand in DCM is also displayed in Figure 2. Three typical absorption peaks at 304 nm, 465 nm and 535 nm were observed for $(CH_3OTPA-BTz-Iq)_2Irpic$. The intense high-lying absorption peak is ascribed to the spin-allowed ligand-central (LC) $\pi-\pi^*$ transitions, the low-lying peak with a shoulder in the region of 400-600 nm can be ascribed to a mixture of 1MLCT , 3MLCT and intramolecular charge transfer (ICT) transitions [45].

The low-energy absorption band cannot be distinctly resolved mainly owing to the hiding of these transitions inside the UV region of the strong singlet transition, which are of much lower but non-negligible absorptivity [30]. Compared to the CH₃OTPA-BTz-Iq free ligand, (CH₃OTPA-BTz-Iq)₂Irp^{ic} exhibited a significantly red-shift low-lying absorption peak, which implies that (CH₃OTPA-BTz-Iq)₂Irp^{ic} with D-A-A architecture has a more intense ICT effect than the CH₃OTPA-BTz-Iq free ligand due to incorporation of the substituent iridium(III) complex acceptor unit [38].

The PL spectra of (CH₃OTPA-BTz-Iq)₂Irp^{ic} in degassed DCM (10⁻⁶ M) at 77 K and 298 K are displayed in Figure 3. As a reference, CH₃OTPA-BTz-Iq in dilute DCM at 298 K is also shown in Figure 3. The corresponding data are summarized in Table 1. At 298 K, under photo-excitation at 460 nm, (CH₃OTPA-BTz-Iq)₂Irp^{ic} exhibits a NIR emission with a strong peak at about 716 nm and a shoulder around 790 nm. At 77 K, the complex displays an additional emission peak at 580 nm, although the strong emission peak and shoulder are very similar to the spectrum at 298 K. In order to further explain the species of the different emission peaks in the spectrum, we measured the lifetimes (τ) at 298 K and 77 K in degassed DCM by using the single-photon counting method. The decay profiles of (CH₃OTPA-BTz-Iq)₂Irp^{ic} at 77 K and 298 K at different emission peaks are shown in Figure S2 (see ESI). At 77 K, (CH₃OTPA-BTz-Iq)₂Irp^{ic} exhibits a much longer emission lifetime of 12.86 μ s at the peak of 580 nm, which can be ascribed to the ligand triplet-triplet emission. Meanwhile, a strong low-temperature phosphorescence band at 708 nm and a shoulder around 783 nm are observed, which shows a little blue shift to the spectrum at 298 K due to the prohibition of the thermal activations [49]. Using Ru(bpy)₃(PF₆)₂ as the standard compound, (CH₃OTPA-BTz-Iq)₂Irp^{ic} shows a fluorescence quantum yield of 0.3% in degassed DCM.

Compared to the iridium (III) complex Ir(tpaiq)₂(acac) (tpa = triphenylamine, iq = isoquinoline, acac = acetoacetone) reported previously by our group [46], the PL spectrum of (CH₃OTPA-BTz-Iq)₂Irp_{ic} presents 80 nm red shift because of an additional A unit (benzotriazole). This indicates that the intramolecular D-A effect is available to make the iridium (III) complexes exhibit red-shifted PL spectra.

3.3 Electrochemical Properties

The redox properties of (CH₃OTPA-BTz-Iq)₂Irp_{ic} were characterized by cyclic voltammetry (CV) method using ferrocene as an internal standard. The recorded voltammograms are shown in Figure S3 and the resulting CV data are summarized in Table 1. An quasi-reversible oxidation wave (E_{ox}) at 0.75 eV and an quasi-reversible reduction wave (E_{red}) at -0.82 eV are observed. According to the reported literature, the oxidation potential is strongly dependent on the electronic environment of the iridium(III) core [47]. On the basis of E_{ox} and E_{red} values, the highest occupied molecular orbital (HOMO) and the lowest unoccupied molecular orbital (LUMO) energy levels (E_{HOMO} and E_{LUMO}) of (CH₃OTPA-BTz-Iq)₂Irp_{ic} are calculated to be -5.08 and -3.5 eV based on the empirical formula, respectively [48]. As the LUMO and HOMO energy levels are -2.20 eV/-5.80 eV for PVK and -2.80 eV/-6.50 eV for OXD-7, (CH₃OTPA-BTz-Iq)₂Irp_{ic} exhibits a matched energy level with the PVK and OXD-7 blend, which is available for (CH₃OTPA-BTz-Iq)₂Irp_{ic} to play a carrier trap role in the PVK-OXD-7-hosted PLEDs. In order to conveniently analyze the energy transfer of the guest and host in the PLEDs, the HOMO-LUMO energy levels of all materials used and the device configuration are shown in Figure 4.

3.5 Electroluminescence Properties

To investigate the applicability of this new emitter in EL devices, a series of spin-coated PLEDs were fabricated with a single-active layer configuration: ITO/

PEDOT:PSS (40 nm)/ PVK:OXD-7 (70:30): x wt% (CH₃OTPA- BTz-Iq)₂Irpic (x =3, 5, 9) (80 nm)/ Ba (4 nm)/ Al (100 nm) (Device I) and a multi-active layer configuration: ITO/ PEDOT:PSS (40 nm)/ PVK:OXD-7 (70:30): x wt% (CH₃OTPA-BTz-Iq)₂Irpic (x = 9, 12, 14, 16) (80 nm)/ TPBI (1,3,5-tri(1-phenyl-1H-benzo[d]imidazol-2-yl)phenyl) (30 nm)/ Ba (4 nm)/ Al (100 nm) (Device II), in which PEDOT was employed as hole-injecting layer (HIL), PVK mixed with OXD-7 was acted as host material because of the PVK has excellent film-forming properties and high hole-transport ability, TPBI was used as the electron-transporting/exciton-blocking layer, and Ba was used as electron-injecting layer (EIL). The doping concentrations in emitting layer were optimized to investigate the device performance. For convenience, devices based on a single-active layer and a multi-active layer are described as I and II, respectively.

Figure 5 shows the EL spectra of the (CH₃OTPA-BTz-Iq)₂Irpic-doped Device I and II at different dopant concentrations. The detailed data are summarized in Table 2. In Device I, at low doping concentration of 3.0 wt%, two distinct EL peaks at about 440 nm and 720 nm with a shoulder peak at about 780 nm were observed, which are assigned to the PVK:OXD-7(70:30) and (CH₃OTPA-BTz-Iq)₂Irpic emissions, respectively. The EL peak of PVK/OXD-7(70:30) is shown in Figure S4. With further increasing dopant concentrations, the PVK:OXD-7 emission was almost quenched and only strong NIR emission from (CH₃OTPA-BTz-Iq)₂Irpic was observed in both Device I and II. This implies that the energy was transferred efficiently from PVK:OXD-7 to (CH₃OTPA-BTz-Iq)₂Irpic. More importantly, we found that the platinum (II) complexes of (TPA-BT-Q)Ptpic and (CH₃OTPA-BTz-Iq)Ptpic, which have the analogous D-A-A structure, displayed a broad, dual EL emission including a strong visible emission (derived from the (TPA-BT-Q) and (CH₃OTPA-BTz-Iq) ligand

center) and NIR emission simultaneously, especially at low dopant concentrations. However, the $(\text{CH}_3\text{OTPA-BTz-Iq})_2\text{Irpic}$ shows no emission of ligand center because the spin-orbit coupling (SOC) strength of iridium(III) complexes are much stronger than that of platinum(II) complexes. (The EL spectra of the three complexes are shown in Figure S5 and Figure S6).

The *EQE* versus current density characteristic of the Device I and II are shown in Figure 6. The corresponding device performance data are summarized in Table 2. In Device I, the maximum *EQE* of 0.20% is observed at the dopant concentrations of 9.0 wt%. Apparently, the *EQEs* tend to decrease firstly and then increase with the increasing dopant ratios in Device I. In Device II, with the use of TPBI, the efficiency enhances significantly because a broader recombination region within the emitting layer is better for carrier balance. The maximum *EQE* of 0.41% at current density of 8.14 mA cm^{-2} is observed at the dopant concentrations of 12.0 wt%. Furthermore, the *EQE* levels display a small roll-off at high current densities. This sluggish efficiency roll-off is favorable for practical applications of OLEDs/PLEDs [49]. Moreover, aside from the octahedral configuration of iridium (III) complexes, the introduction of bulky nonplanar TPA unit into $(\text{CH}_3\text{OTPA-BTz-Iq})_2\text{Irpic}$ can also effectively reduce the chances of π -stacking of dopants [38].

The current densities (*J*)-voltage (*V*)-radiance (*R*) characteristics of the $(\text{CH}_3\text{OTPA-BTz-Iq})_2\text{Irpic}$ doped Device I and II are shown in Figure 7 and their corresponding data are summarized in Table 2. Device II acquired a preferable performance with a radiant emittance of $74.1 \mu\text{W cm}^{-2}$ at 23.2 mA cm^{-2} and 12.0 wt% doping concentrations.

4. Conclusions

In summary, a novel benzotriazole-containing D-A-A type cyclometalated iridium (III) complex of $(\text{CH}_3\text{OTPA-BTz-Iq})_2\text{Irpic}$ was obtained with a NIR-EL emission peak at 723 nm and a shoulder at 780 nm. Its NIR-emitting PLEDs showed a suppressed efficiency roll-off with increasing operating current densities. The best device performances were presented in the device at 12.0 wt% dopant concentration in Decive II. The maximum *EQE* of 0.41% at 8.14 mA cm^{-2} and an irradiance intensity of $74.1 \mu\text{W cm}^{-2}$ at 23.2 V were observed. This work indicates that introducing appropriate D and A unit to develop D-A-A structure is an efficient approach to construct high-efficiency NIR-emitting iridium (III) complex in PLEDs with insignificant efficiency roll-off.

Acknowledgements

This work was supported by Scientific Research Fund of Hunan Provincial Education Department (15C0531), the National Natural Science Foundation of China (51473140), the Natural Science Foundation of Hunan University of Science and Technology (E51522) and the Open Project Program of Key Laboratory of Theoretical Organic Chemistry and Functional Molecule, Ministry of Education (E21507).

References

- [1] Chen H, Lin W, Cui H, Jiang W. Development of unique xanthene-cyanine fused near-infrared fluorescent fluorophores with superior chemical stability for biological fluorescence imaging. *Chem-Eur J.* 2015;21:733-45.
- [2] Guo Z, Park S, Yoon J, Shin I. Recent progress in the development of near-infrared fluorescent probes for bioimaging applications. *Chem Soc Rev.* 2014;43:16-29.
- [3] Xiang H, Cheng J, Ma X, Zhou X, Chruma JJ. Near-infrared phosphorescence: materials and applications. *Chem Soc Rev.* 2013;42:6128-85.
- [4] Qian G, Wang ZY. Near-infrared organic compounds and emerging applications. *Chem Asian J.* 2010;5:1006-29.
- [5] Ho C-L, Li H, Wong W-Y. Red to near-infrared organometallic phosphorescent dyes for OLED applications. *J Organomet Chem.* 2014;751:261-85.
- [6] Artizzu F, Mercuri ML, Serpe A, Deplano P. NIR-emissive erbium–quinolinolate complexes. *Coord Chem Rev.* 2011;255:2514-29.
- [7] Chen Z-Q, Ding F, Bian Z-Q, Huang C-H. Efficient near-infrared organic light-emitting diodes based on multimetallic assemblies of lanthanides and iridium complexes. *Org Electron.* 2010;11:369-76.
- [8] Katkova MA, Pushkarev AP, Balashova TV, Konev AN, Fukin GK, Ketkov SY, et al. Near-infrared electroluminescent lanthanide [Pr(iii), Nd(iii), Ho(iii), Er(iii), Tm(iii), and Yb(iii)] N,O-chelated complexes for organic light-emitting devices. *J Mater Chem.* 2011;21:16611-20.
- [9] Yao L, Zhang S, Wang R, Li W, Shen F, Yang B, et al. Highly efficient near-infrared organic light-emitting diode based on a butterfly-shaped donor-acceptor chromophore with strong solid-state fluorescence and a large proportion of radiative

- excitons. *Angew Chem Int Ed.* 2014;53:2119-23.
- [10] Ellinger S, Graham KR, Shi P, Farley RT, Steckler TT, Brookins RN, et al. Donor-acceptor-donor-based π -conjugated oligomers for nonlinear optics and near-IR emission. *Chem Mater.* 2011;23:3805-17.
- [11] Du X, Qi J, Zhang Z, Ma D, Wang ZY. Efficient non-doped near infrared organic light-emitting devices based on fluorophores with aggregation-induced emission enhancement. *Chem Mater.* 2012;24:2178-85.
- [12] Qian G, Zhong Z, Luo M, Yu D, Zhang Z, Wang ZY, et al. Simple and efficient near-infrared organic chromophores for light-emitting diodes with single electro-luminescent emission above 1000 nm. *Adv Mater.* 2009;21:111-6.
- [13] Luo J, Hou Q, Chen J, Cao Y. Luminescence and photovoltaic cells of benzo-selenadiazole-containing polyfluorenes. *Synth Met.* 2006;156:470-5.
- [14] Steckler TT, Fenwick O, Lockwood T, Andersson MR, Cacialli F. Near-infrared polymer light-emitting diodes based on low-energy gap oligomers copolymerized into a high-gap polymer host. *Macromol Rapid Commun.* 2013;34:990-6.
- [15] Chongjun J, Kuo-Wei H, Jishan W. Perylene-fused BODIPY dye with near-IR absorption/emission and high photostability. *Org Lett.* 2011;13:632-5.
- [16] Wang J, Wu Q, Wang S, Yu C, Li J, Hao E, et al. Conformation-restricted partially and fully fused BODIPY dimers as highly stable near-infrared fluorescent dyes. *Org Lett.* 2015;17:5360-3.
- [17] Zhang X, Yu H, Xiao Y. Replacing phenyl ring with thiophene: an approach to longer wavelength aza-dipyrromethene boron difluoride (Aza-BODIPY) dyes. *J Org Chem.* 2012;77:669-73.
- [18] Ma X, Mao X, Zhang S, Huang X, Cheng Y, Zhu C. Aza-BODIPY-based D- π -A conjugated polymers with tunable band gap: synthesis and near-infrared emission.

Polym Chem. 2013;4:520-7.

[19] Wang Y, Chen J, Zhen Y, Jiang H, Yu G, Liu Y, et al. Synthesis and properties of novel near-infrared dye based on BODIPY and diketopyrrolopyrrole units. *Mater Lett.* 2015;139:130-3.

[20] Williams EL, Li J, Jabbour GE. Organic light-emitting diodes having exclusive near-infrared electrophosphorescence. *Appl Phys Lett.* 2006;89:083506.

[21] Cocchi M, Virgili D, Fattori V, Williams JAG, Kalinowski J. Highly efficient near-infrared organic excimer electrophosphorescent diodes. *Appl Phys Lett.* 2007;90:023506.

[22] Cocchi M, Kalinowski J, Virgili D, Williams JAG. Excimer-based red/near-infrared organic light-emitting diodes with very high quantum efficiency. *Appl Phys Lett.* 2008;92:113302.

[23] Lee T-C, Hung J-Y, Chi Y, Cheng Y-M, Lee G-H, Chou P-T, et al. Rational design of charge-neutral, near-infrared-emitting osmium(II) complexes and OLED fabrication. *Adv Funct Mater.* 2009;19:2639-47.

[24] Wu X, Liu Y, Wang Y, Wang L, Tan H, Zhu M, et al. Highly efficient near-infrared emission from binuclear cyclo-metalated platinum complexes bridged with 5-(4-octyloxyphenyl)-1,3,4-oxadiazole-2-thiol in PLEDs. *Org Electron.* 2012;13:932-7.

[25] Graham KR, Yang Y, Sommer JR, Shelton AH, Schanze KS, Xue J, et al. Extended conjugation platinum(II) porphyrins for use in near-infrared emitting organic light emitting diodes. *Chem Mater.* 2011;23:5305-12.

[26] Borek C, Hanson K, Djurovich PI, Thompson ME, Aznavour K, Bau R, et al. Highly efficient, near-infrared electrophosphorescence from a Pt-metalloporphyrin complex. *Angew Chem Int Ed.* 2007;46:1109-12.

- [27] Qiao J, Duan L, Tang L, He L, Wang L, Qiu Y. High-efficiency orange to near-infrared emissions from bis-cyclometalated iridium complexes with phenylbenzoquinoline isomers as ligands. *J Mater Chem*. 2009;19:6573-80.
- [28] Tao R, Qiao J, Zhang G, Duan L, Chen C, Wang L, et al. High-efficiency near-infrared organic light-emitting devices based on an iridium complex with negligible efficiency roll-off. *J Mater Chem C*. 2013;1:6446-54.
- [29] Tao R, Qiao J, Zhang G, Duan L, Wang L, Qiu Y. Efficient near-infrared-emitting cationic iridium complexes as dopants for OLEDs with small efficiency roll-off. *J Phys Chem C*. 2012;116:11658-64.
- [30] Ho C-L, Yao B, Zhang B, Wong K-L, Wong W-Y, Xie Z, et al. Metallophosphors of iridium(III) containing borylated oligothiophenes with electroluminescence down to the near-infrared region. *J Organomet Chem*. 2013;730:144-55.
- [31] Cao X, Miao J, Zhu M, Zhong C, Yang C, Wu H, et al. Near-infrared polymer light-emitting diodes with high efficiency and low efficiency roll-off by using solution-processed iridium(III) phosphors. *Chem Mater*. 2015;27:96-104.
- [32] Xin L, Xue J, Lei G, Qiao J. Efficient near-infrared-emitting cationic iridium complexes based on highly conjugated cyclometalated benzo[g]phthalazine derivatives. *Rsc Adv*. 2015;5:42354-61.
- [33] Kesarkar S, Mróz W, Penconi M, Pasini M, Destri S, Cazzaniga M, et al. Near-IR emitting iridium(III) complexes with heteroaromatic β -diketonate ancillary ligands for efficient solution-processed OLEDs: structure-property correlations. *Angew. Chem. Int. Ed*. 2016;55:2714-8.
- [34] Su N, Meng F, Chen J, Wang Y, Tan H, Su S, et al. Near-infrared emitting pyrazole-bridged binuclear platinum complexes: synthesis, photophysical and electroluminescent properties in PLEDs. *Dyes Pigments*. 2016;128:68-74.

- [35] Baldo MA, O'Brien DF, You Y, Shoustikov A, Sibley S, Thompson ME, et al. Highly efficient phosphorescent emission from organic electroluminescent devices. *Nature*. 1998;395:151-4.
- [36] Tao P, Li W-L, Zhang J, Guo S, Zhao Q, Wang H, et al. Facile synthesis of highly efficient lepidine-based phosphorescent iridium(III) complexes for yellow and white organic light-emitting diodes. *Adv. Funct. Mater.* 2016;26:881-94.
- [37] Xie LH, Zhu R, Qian Y, Liu RR, Chen SF, Lin J, et al. Spiro-functionalized ligand with supramolecular steric hindrance to control π - π interaction in the iridium complex for high-performance electrophosphorescent devices. *J Phys Chem Lett.* 2009;1:272-6.
- [38] Yu J, He K, Li Y, Tan H, Zhu M, Wang Y, et al. A novel near-infrared-emitting cyclometalated platinum (II) complex with donor-acceptor-acceptor chromophores. *Dyes Pigments.* 2014;107:146-52.
- [39] Price SC, Stuart AC, Yang L, Zhou H, You W. Fluorine substituted conjugated polymer of medium band gap yields 7% efficiency in polymer-fullerene solar cells. *J Am Chem Soc.* 2011;133:4625-31.
- [40] Tomkute-Luksiene D, Keruckas J, Malinauskas T, Simokaitiene J, Getautis V, Grazulevicius JV, et al. 2-Phenyl-1,2,3-benzotriazole Ir(III) complexes with additional donor fragment for single-layer PhOLED devices. *Dyes Pigments.* 2013;96: 278-86.
- [41] Xia Z-Y, Xiao X, Su J-H, Chang C-S, Chen CH, Li D-L, et al. Low driving voltage and efficient orange-red phosphorescent organic light-emitting devices based on a benzotriazole iridium complex. *Synth Met.* 2009;159:1782-5.
- [42] Malinauskas T, Daskeviciene M, Kazlauskas K, Su H-C, Grazulevicius JV, Jursenas S, et al. Multifunctional red phosphorescent bis-cyclometallated iridium complexes based on 2-phenyl-1,2,3-benzotriazole ligand and carbazolyl moieties.

Tetrahedron. 2011;67:1852-61.

[43] Balan A, Baran D, Toppare L. Benzotriazole containing conjugated polymers for multipurpose organic electronic applications. *Polym Chem.* 2011;2:1029-43.

[44] Li Jian, Djurovich PI, Alleyne BD, Yousufuddin M, Ho NN, Thomas JC, Peters JC, Rand B, Thompson ME. Synthetic control of excited-state properties in cyclometalated Ir(III) complexes using ancillary ligands. *Inorg Chem* 2005; 44: 1713-26.

[45] Youngmin Y, Soo Young P. Inter-ligand energy transfer and related emission change in the cyclometalated heteroleptic iridium complex: facile and efficient color tuning over the whole visible range by the ancillary ligand structure. *J Am Chem Soc.* 2005;127:12438-9.

[46] Hu Z, Luo C, Wang L, Huang F, Zhu K, Wang Y, et al. Highly efficient saturated red electrophosphorescence from isoquinoline-based iridium complex containing triphenylamino units in polymer light-emitting devices. *Chem Phys Lett.* 2007;441: 277-81.

[47] Schneidenbach D, Ammermann S, Debeaux M, Freund A, Zollner M, Daniliuc C, et al. Efficient and long-time stable red iridium(III) complexes for organic light-emitting diodes based on quinoxaline ligands. *Inorg Chem.* 2010;49:397-406.

[48] Dou L, Gao J, Richard E, You J, Chen CC, Cha KC, et al. Systematic investigation of benzodithiophene- and diketopyrrolopyrrole-based low-bandgap polymers designed for single junction and tandem polymer solar cells. *J Am Chem Soc.* 2012;134:10071-9.

[49] Karatsu T, Takahashi M, Yagai S, Kitamura A. Photophysical properties of substituted homoleptic and heteroleptic phenylimidazolinato Ir(III) complexes as a blue phosphorescent material. *Inorg Chem.* 2013;52:12338-50.

Captions of Figures

Figure 1 Molecular structure of $(\text{CH}_3\text{OTPA-BTz-Iq})_2\text{Irpic}$

Scheme 1 Synthetic route of $(\text{CH}_3\text{OTPA-BTz-Iq})_2\text{Irpic}$

Figure 2 Normalized UV-vis absorption spectra of $\text{CH}_3\text{OTPA-BTz-Iq}$ ligand and $(\text{CH}_3\text{OTPA-BTz-Iq})_2\text{Irpic}$ in DCM at 298 K

Figure 3 Normalized PL spectra of $\text{CH}_3\text{OTPA-BTz-Iq}$ ligand in deaerated DCM at 298 K and $(\text{CH}_3\text{OTPA-BTz-Iq})_2\text{Irpic}$ in deaerated DCM at 298 K and 77 K

Figure 4 Energy level diagram and device structure of the $(\text{CH}_3\text{OTPA-BTz-Iq})_2\text{Irpic}$ -doped PLEDs

Figure 5 EL spectra of the $(\text{CH}_3\text{OTPA-BTz-Iq})_2\text{Irpic}$ -doped PLEDs. (a) EL spectra in Device I at dopant concentrations from 3 wt % to 9 wt%; (b) EL spectra in Device II at dopant concentrations from 9 wt% to 16 wt%.

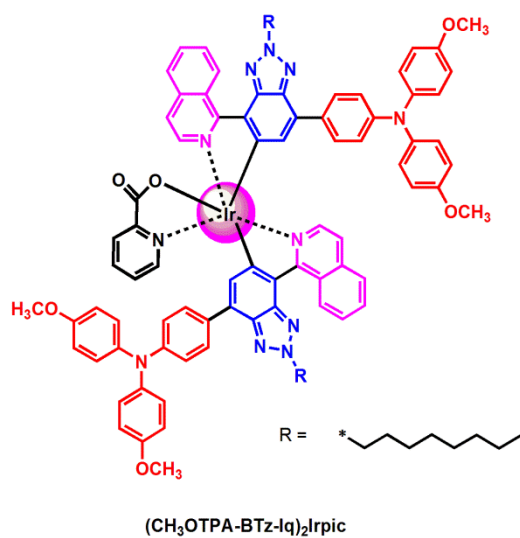
Figure 6 The *EQE* versus current density characteristics of Device I (a) and Device II (b).

Figure 7 The current density-voltage-radiance (*J-V-R*) curves of the $(\text{CH}_3\text{OTPA-BTz-Iq})_2\text{Irpic}$ -doped devices at different concentrations: (a) from 3 wt% to 9 wt% in Device I; (b) from 9 wt% to 16 wt% in Device II.

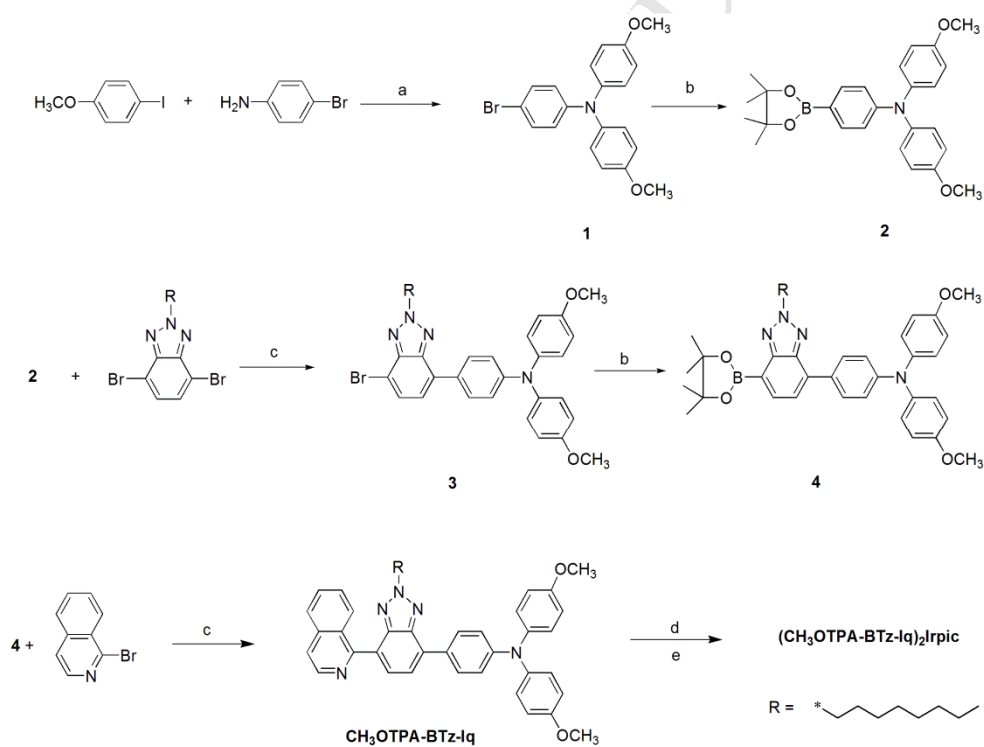
Table 1 Photophysical and electrochemical properties of $(\text{CH}_3\text{OTPA-BTz-Iq})_2\text{Irpic}$

Table 2 The EL parameters of the $(\text{CH}_3\text{OTPA-BTz-Iq})_2\text{Irpic}$ -doped PLEDs

Figure 1



Scheme 1



(a) 1,10-phenanthroline anhydrous, CuI, KOH, toluene (b) KOAc, Pd(dppf)Cl₂, bis(pinacolato)diboron, anhydrous THF (c) K₂CO₃, Pd(PPh₃)₄, toluene, methanol (d) picolinic acid, 2-ethoxyethanol, Na₂CO₃ (e) IrCl₃ H₂O, 2-ethoxyethanol, H₂O

Figure 2

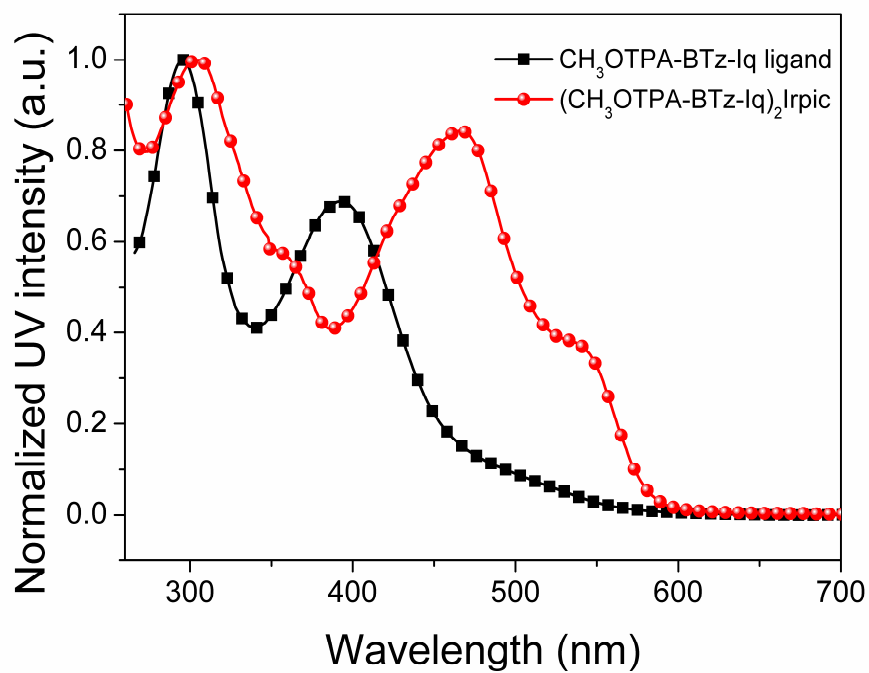


Figure 3

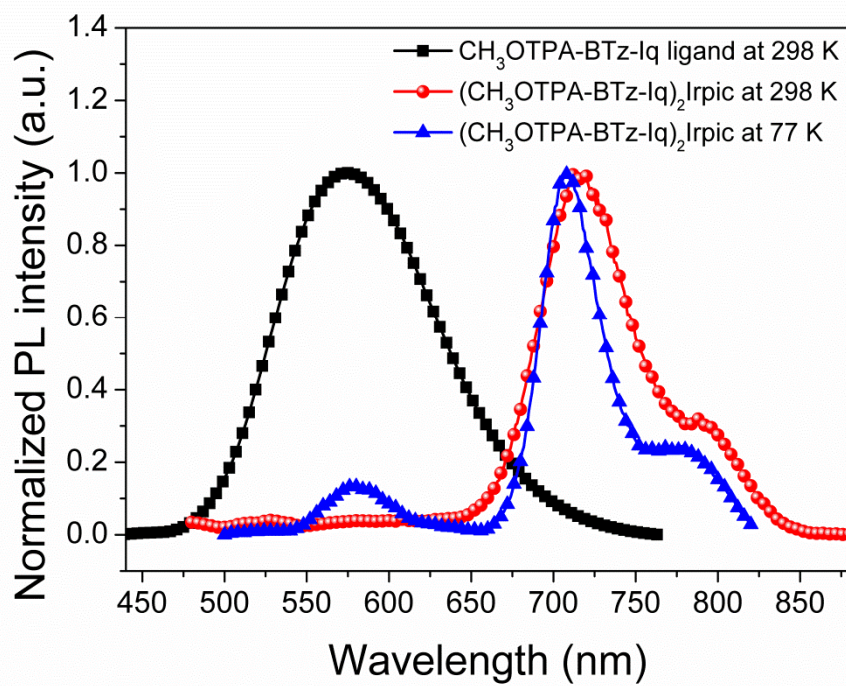


Figure 4

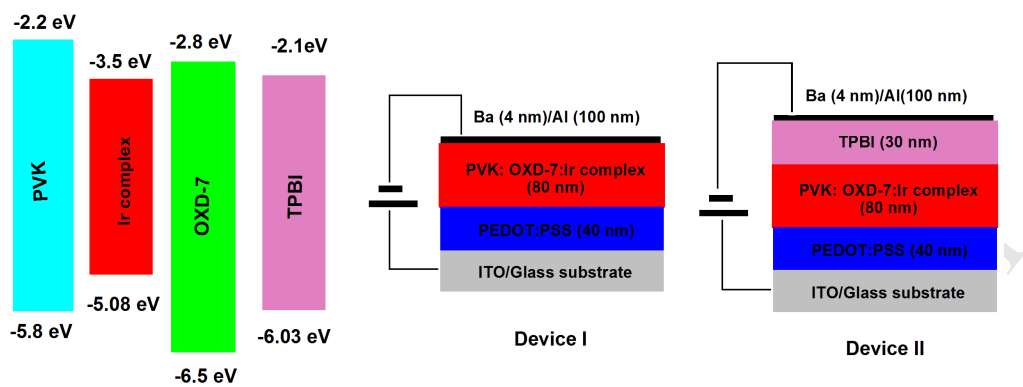


Figure 5

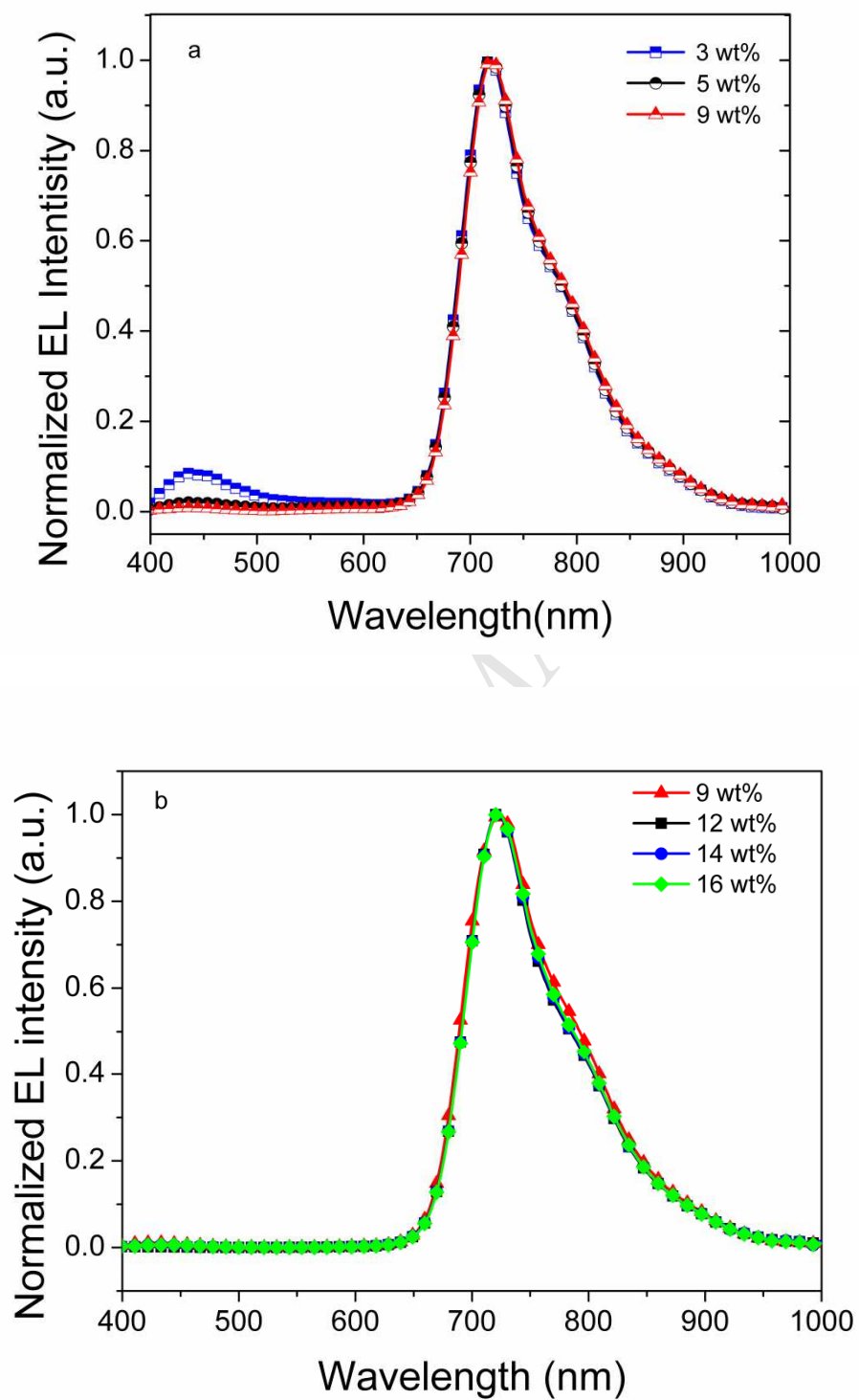


Figure 6

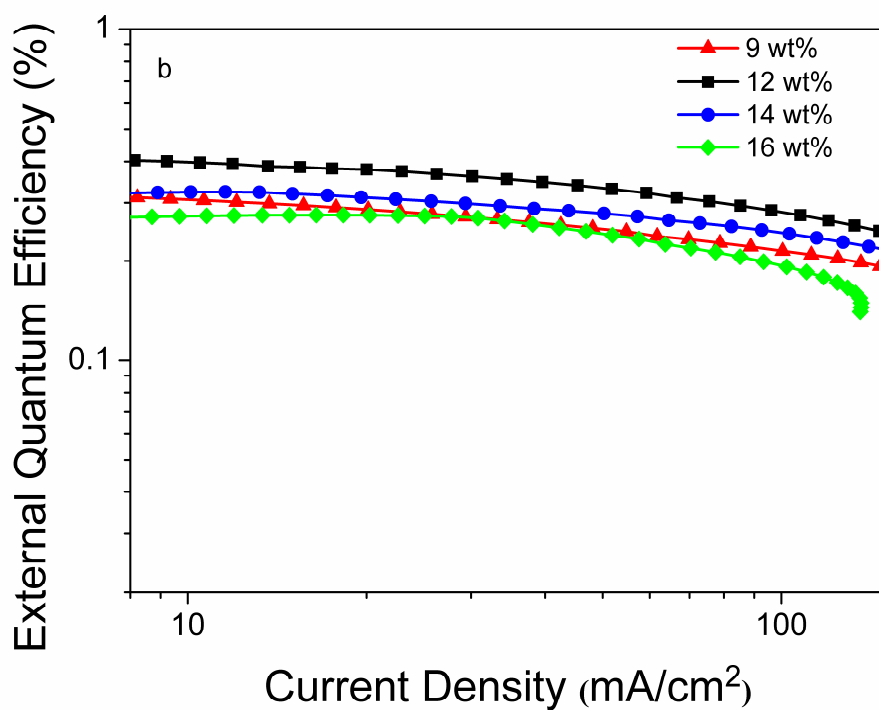
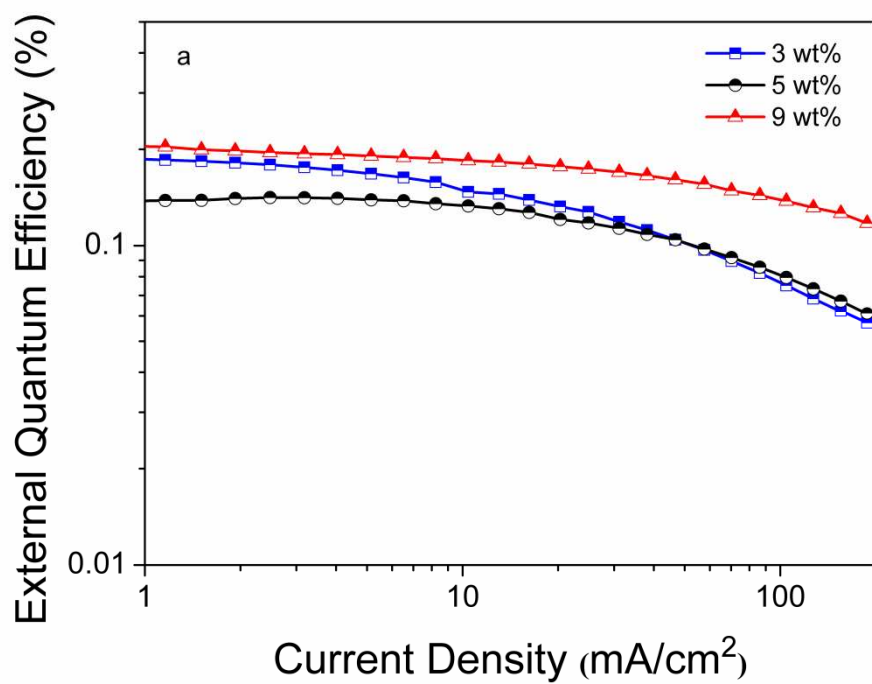


Figure 7

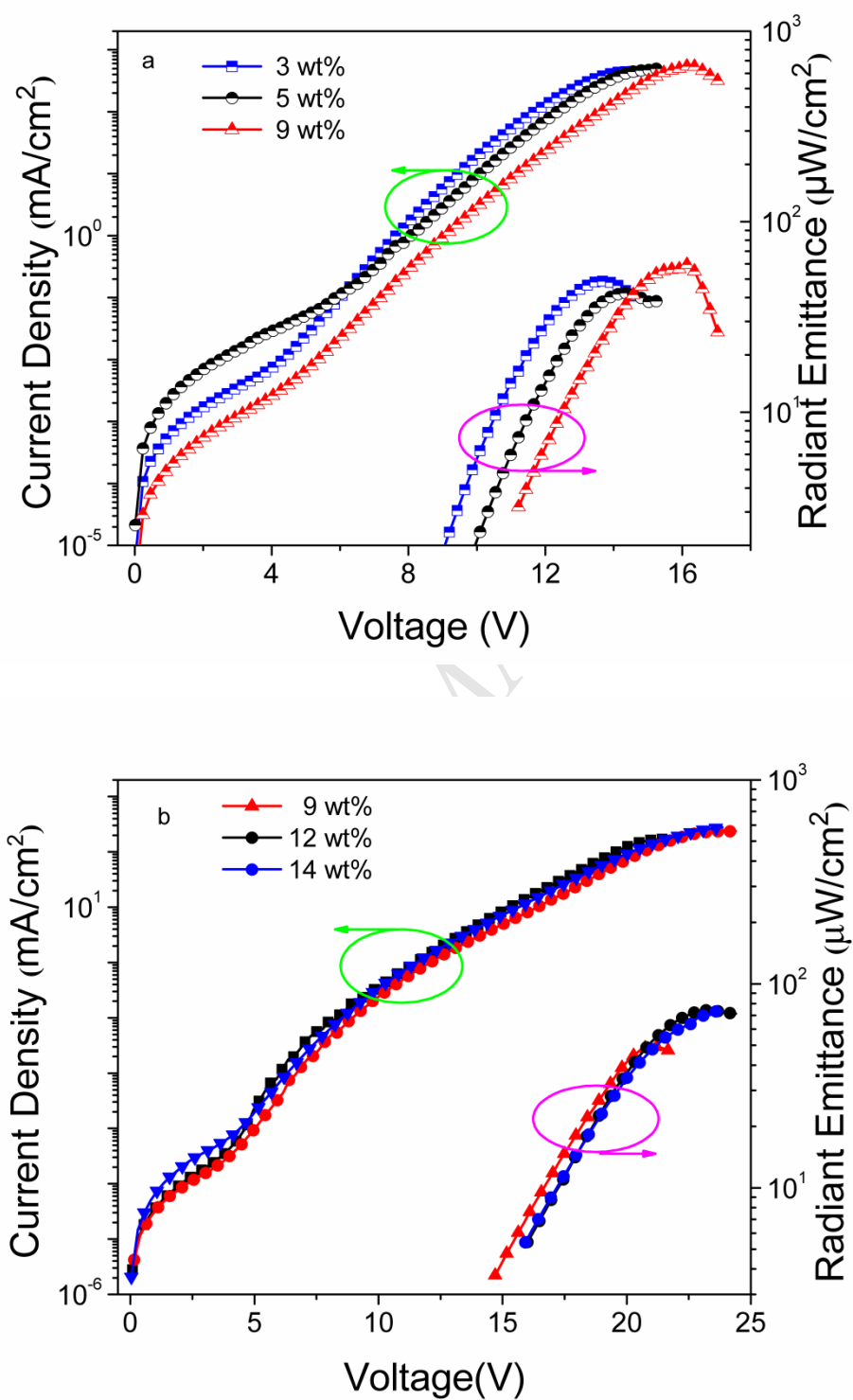


Table 1

UV-vis $\lambda/\text{nm}^{\text{a}}$ ($\epsilon_{\text{max}}/\text{L mol}^{-1}\text{cm}^{-1}$) ^b	PL λ/nm ($\tau/\mu\text{s}$) ^a		$E_{\text{T}}/\text{eV}^{\text{c}}$	E_{HOMO} /eV ^d	E_{LUMO} /eV ^d	E_{g} /eV
	77 K	298 K				
304(153389),	580(12.86),	718(0.48),				
465(129269),	708(2.80),	790(0.47)	1.75	-5.08	-3.50	1.58
535(56174)	783(2.54)					

^a Measured in DCM at 298 K at a concentration of 10^{-6} mol L⁻¹.

^b Molar extinction coefficient at 298 K.

^c Triplet energy was deduced from the highest peak of phosphorescent.

^d $E_{\text{HOMO}} = -(4.33 + E_{\text{ox}})$ eV, $E_{\text{LUMO}} = -(4.33 + E_{\text{red}})$ eV

Table 2

dopant ratio (wt%)	device type	λ_{EL} (nm) ^a	EQE_{max} (%) ^b	J (mA cm ⁻²) ^c	R_{max} ($\mu\text{W cm}^{-2}$) [V at R_{max} (V)]
3	I	440, 719, 780(sh)	0.18	1.92	48.6 (13.6)
5	I	719, 780(sh)	0.14	3.17	42.2 (14.3)
9	I	719, 780(sh)	0.20	1.16	59.5 (16.1)
9	II	723, 780(sh)	0.31	7.16	49.2 (20.9)
12	II	723, 780(sh)	0.41	8.14	74.1 (23.2)
14	II	723, 780(sh)	0.32	7.79	43.5 (23.8)
16	II	723, 780(sh)	0.27	7.81	not measured

sh=shoulder

^a λ_{EL} : the maximum EL emission peak

^b EQE_{max} : the maximum external quantum efficiency

^c current density at EQE_{max}

Supporting Information to:

Benzotriazole-containing Donor-Acceptor-Acceptor Type Cyclometalated Iridium(III)

Complex for Solution-processed Near-infrared Polymer Light Emitting Diodes

Junting Yu,^{a*} Hua Tan,^b Fanyuan Meng,^b Kun Lv,^a Weiguo Zhu,^{b*} and Shijian Su^{c*}

^a Key Laboratory of Theoretical Organic Chemistry and Functional Molecule,
Ministry of Education, College of Chemistry and Chemical Engineering, Hunan
University of Science and Technology, Xiangtan 411201, P. R. China

^b College of Chemistry, Key Lab of Environment-Friendly Chemistry and Application
in the Ministry of Education, Xiangtan University, Xiangtan 411105, P. R. China

^c Institute of Polymer Optoelectronic Materials and Devices, South China University
of Technology, Guangzhou 510640, P. R. China

Figure S1. TGA curve of $(\text{CH}_3\text{OTPA-BTz-Iq})_2\text{Irpic}$ under a stream of nitrogen at a scanning rate of $20\text{ }^\circ\text{C min}^{-1}$

Figure S2. Decay profile of $(\text{CH}_3\text{OTPA-BTz-Iq})_2\text{Irpic}$ at 77 K and 298 K at different emission peak.

Figure S3. Cyclic voltammogram of the $(\text{CH}_3\text{OTPA-BTz-Iq})_2\text{Irpic}$.

Figure S4. The EL spectra of the host material PVK:OXD-7(70:30)

Figure S5. The EL spectra of the $(\text{CH}_3\text{OTPA-BTz-Iq})\text{Ptpic}$ -doped PLEDs at dopant concentrations from 1 wt % to 9 wt%.

Figure S6. The EL spectra of the $(\text{CH}_3\text{OTPA-BTz-Iq})_2\text{Irpic}$ - and $(\text{TPA-BT-Q})\text{Ptpic}$ -doped PLEDs at 8 wt% and 9 wt% doping concentrations, respectively.

Figure S7. ^1H NMR and MALDI-TOF mass spectra of $\text{CH}_3\text{OTPA-BTz-Iq}$ and $(\text{CH}_3\text{OTPA-BTz-Iq})_2\text{Irpic}$

Figure S1

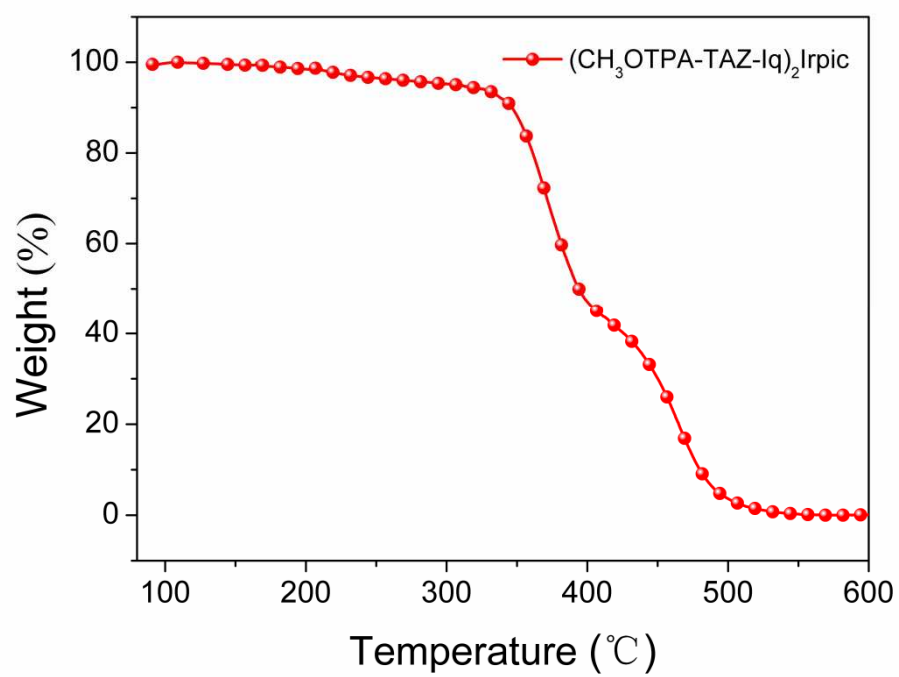


Figure S2

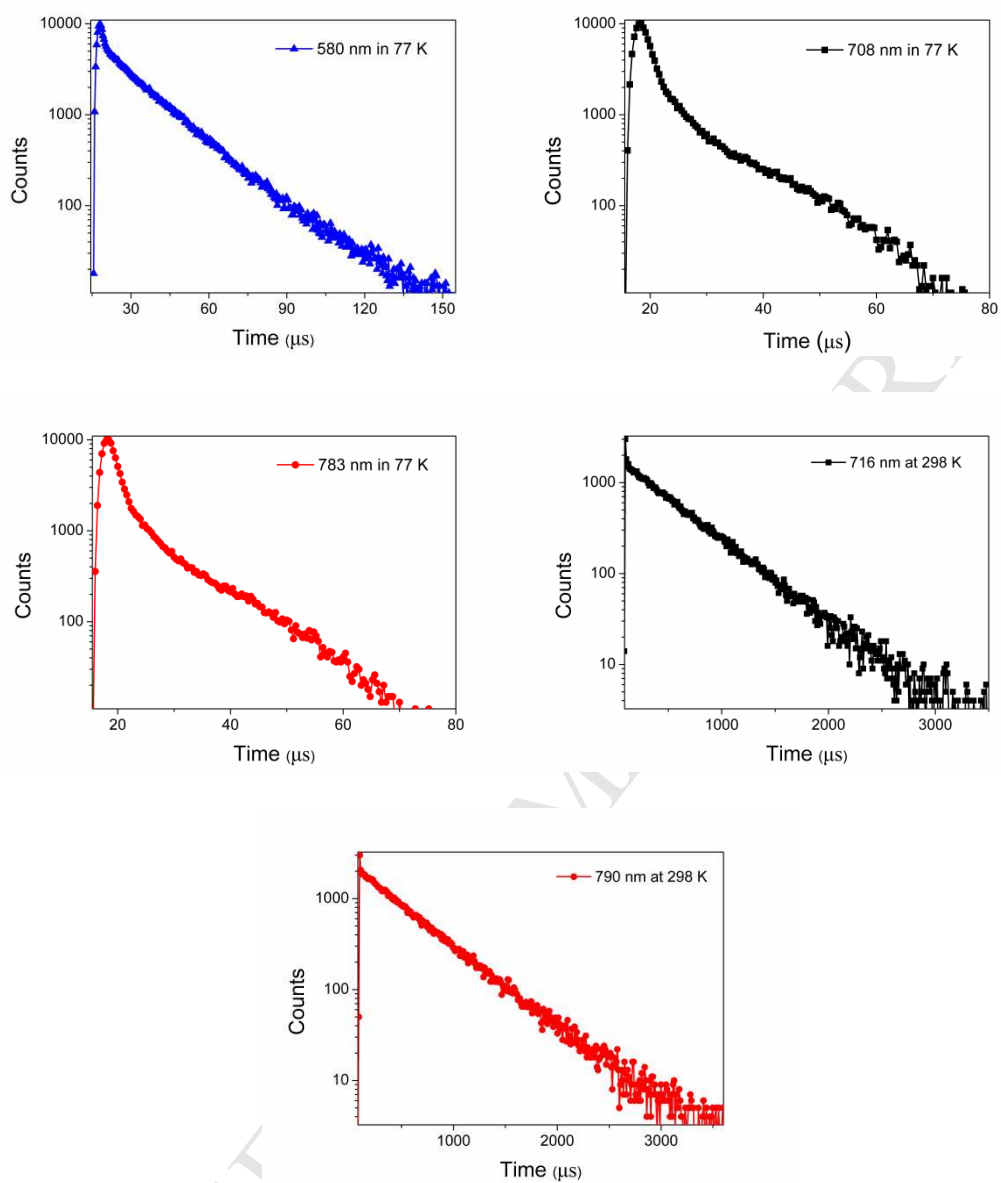


Figure S3

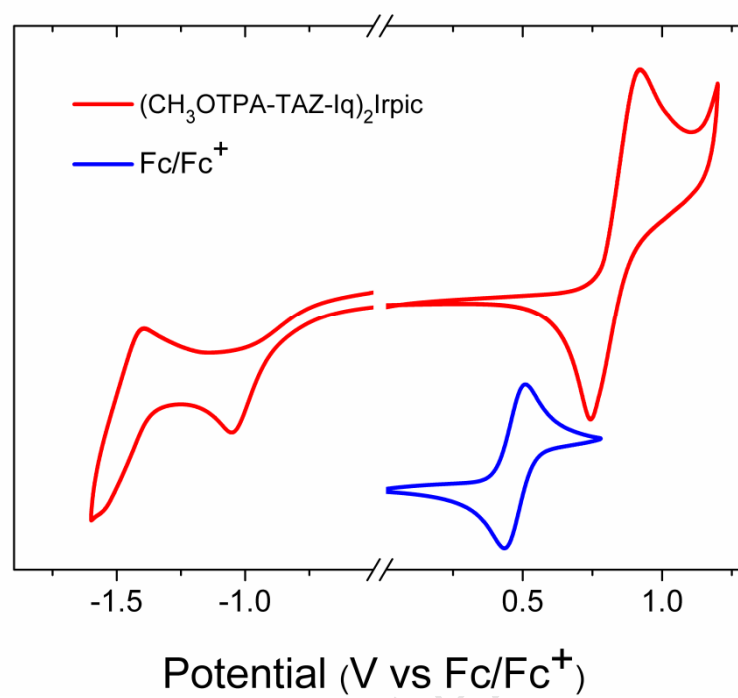


Figure S4

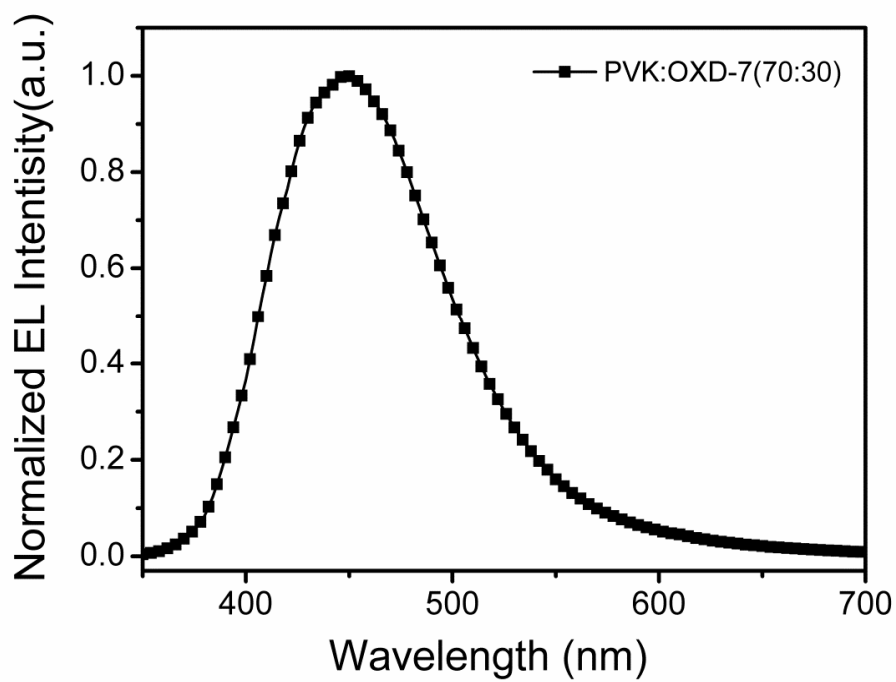


Figure S5

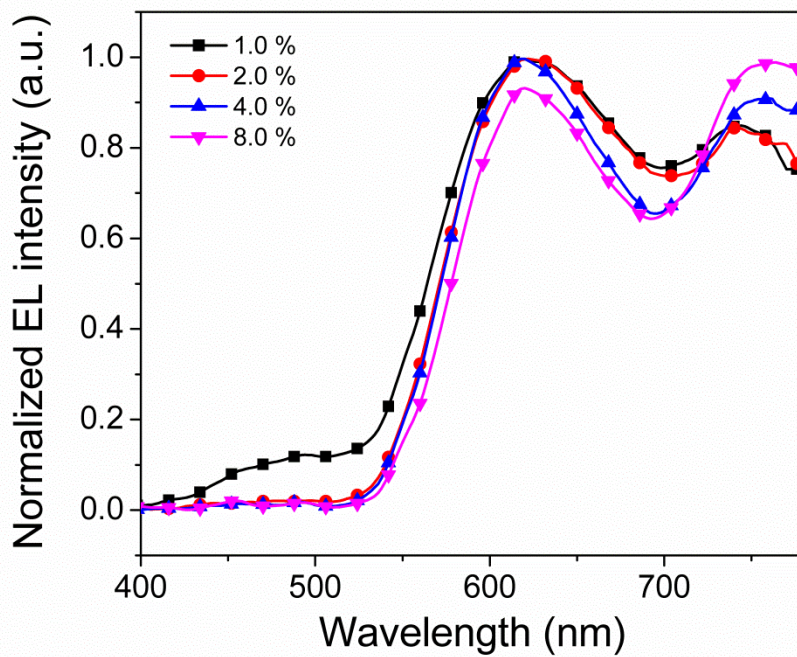


Figure S6

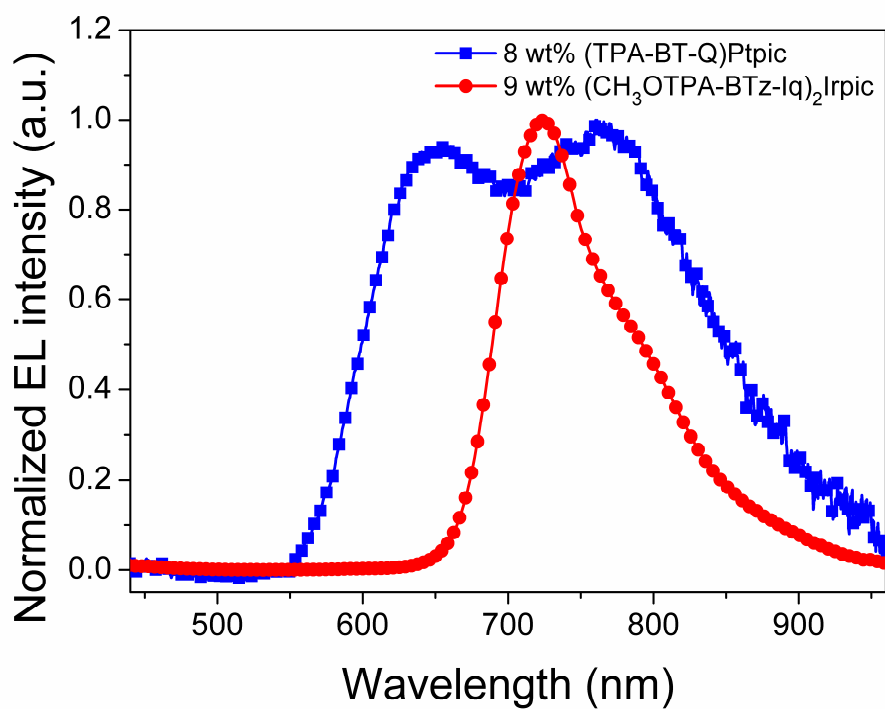
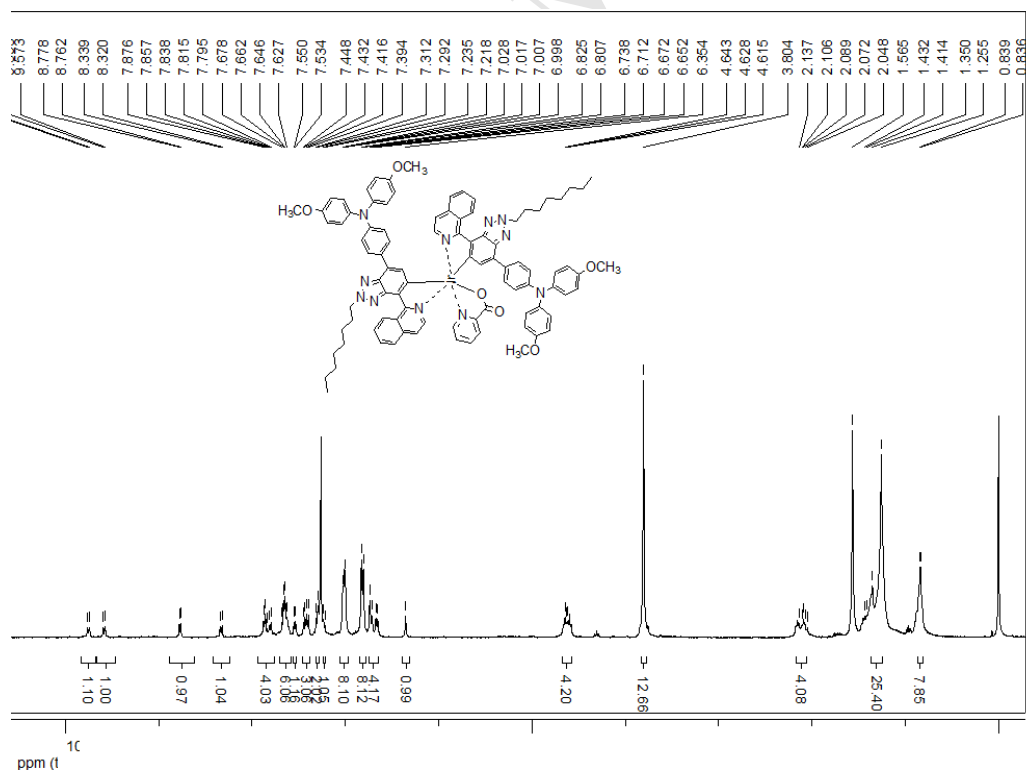
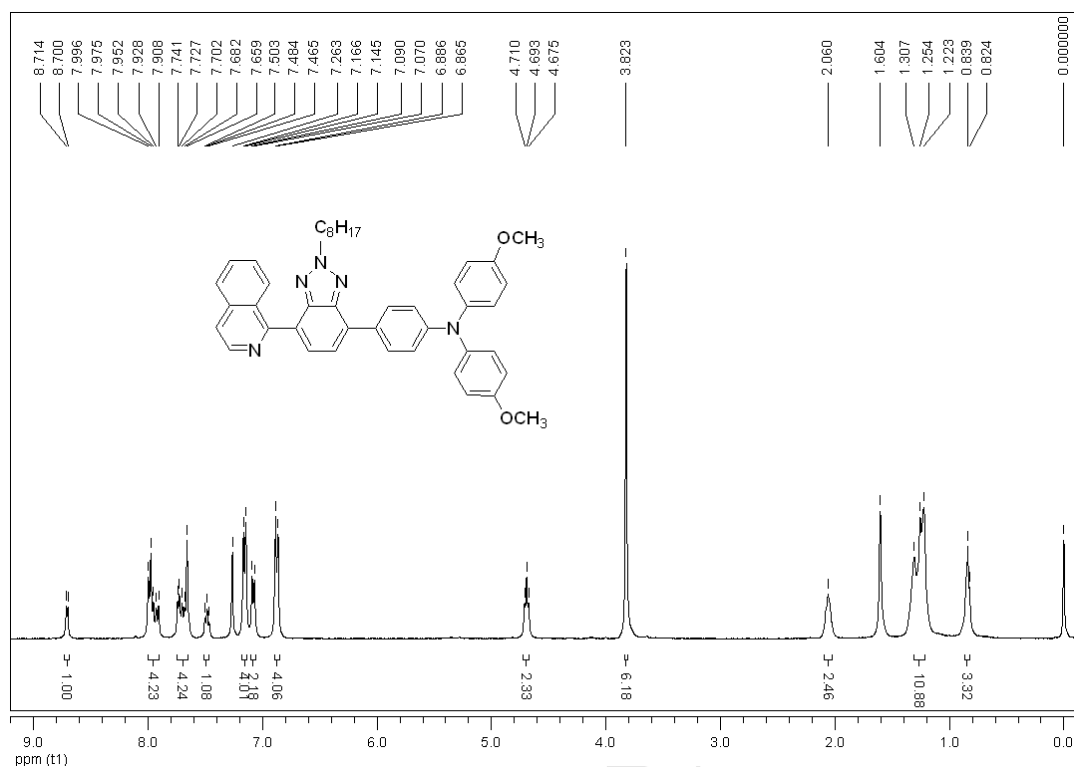
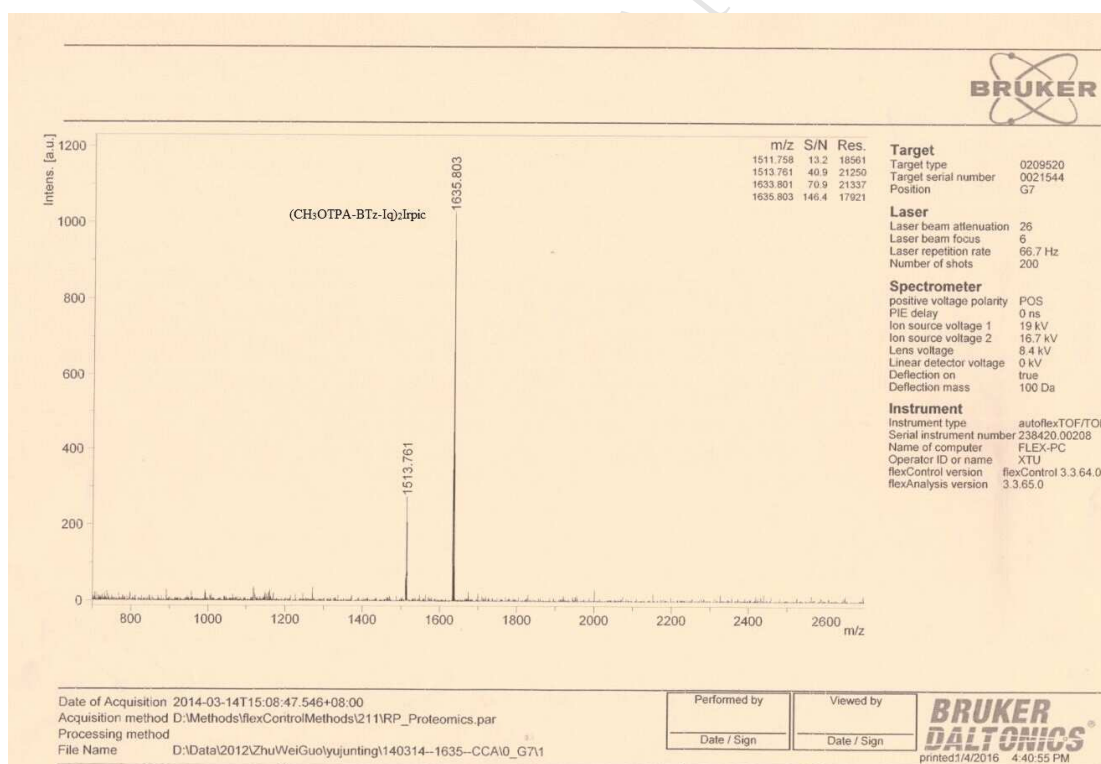
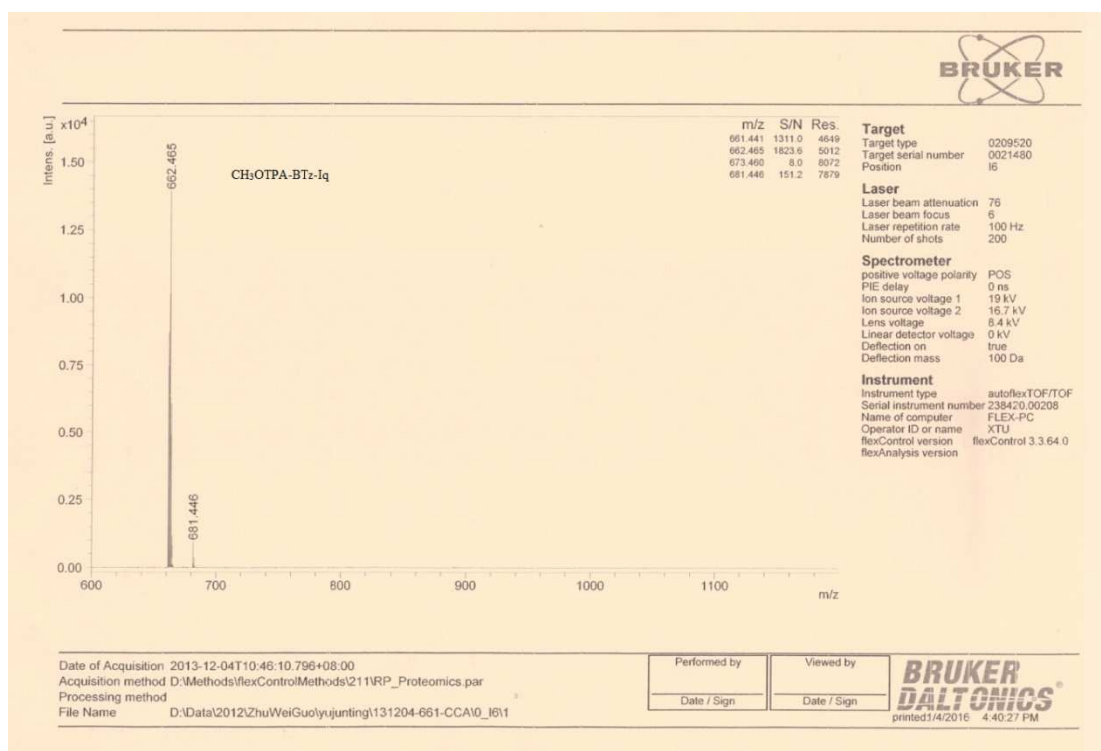


Figure S7





Highlights

- A novel iridium(III) complex of (CH₃OTPA-BTz-Iq)₂Irpic with a D-A-A structure was synthesized.
- The (CH₃OTPA-BTz-Iq)₂Irpic shows an emission at 718 nm and a shoulder at 790 nm in solution at 298 K.
- The (CH₃OTPA-BTz-Iq)₂Irpic-doped PLEDs exhibited a near-infrared EL emission peaked at 723 nm.
- The maximum *EQE* of 0.41% and a radiant intensity of 74.1 $\mu\text{W cm}^{-2}$ were obtained in their doped PLEDs.